



# Optics Letters

## Side-excitation light-induced thermoelastic spectroscopy

QIAN WU,<sup>1</sup> HAOHUA LV,<sup>1</sup> JUNMING LI,<sup>1</sup> ZHIFEI YANG,<sup>1</sup> RUIFENG KAN,<sup>2</sup> MARILENA GIGLIO,<sup>3</sup>   
WENGUO ZHU,<sup>1</sup> YONGCHUN ZHONG,<sup>1</sup> ANGELO SAMPAOLO,<sup>3</sup> PIETRO PATIMISCO,<sup>3</sup> VINCENZO  
SPAGNOLO,<sup>3,4</sup> JIANHUI YU,<sup>1</sup> AND HUADAN ZHENG<sup>1,\*</sup>

<sup>1</sup>Guangdong Provincial Key Laboratory of Optical Fiber Sensing and Communications, and Department of Optoelectronic Engineering, Jinan University, Guangzhou 510632, China

<sup>2</sup>Key Laboratory of Environmental Optics and Technology, Anhui Institute of Optics and Fine Mechanics, Chinese Academy of Sciences, Hefei, Anhui 230031, China

<sup>3</sup>PolySense Lab, Dipartimento Interateneo di Fisica, University and Politecnico of Bari, CNR-IFN, Via Amendola 173, Bari 70126, Italy

<sup>4</sup>e-mail: vincenzoluigi.spagnolo@poliba.it

\*Corresponding author: zhenghuadan@jnu.edu.cn

Received 18 October 2022; revised 5 December 2022; accepted 11 December 2022; posted 20 December 2022; published 17 January 2023

**In this Letter, a side-excitation light-induced thermoelastic spectroscopy (SE-LITES) technique was developed for trace gas detection. A novel, to the best of our knowledge, custom quartz tuning fork (QTF) was used as a transducer for photon detection by the thermoelastic effect. The mechanical stress distribution on the QTF surface was analyzed to identify the optimum thermoelastic excitation approach. The electrode film on the QTF surface also works as a partially reflective layer to obtain a long optical absorption path inside the QTF body. With the long optical absorption length and the inner face excitation of the QTF, the thermoelastic effect was greatly enhanced. With an optimized modulation depth, a signal-to-noise ratio (SNR) improvement of more than one order of magnitude was achieved, compared to traditional LITES.** © 2023 Optica Publishing Group

<https://doi.org/10.1364/OL.478630>

Photoacoustic (PA) and photothermal (PT) spectroscopies have shown great potential in trace gas detection due to their advantages in high sensitivity, compact structure, and wide dynamic range [1–5]. Compared to other gas sensing spectroscopic methods, the main advantage of PAS and PTS is that the detection sensitivity does not rely on the optical absorption length, thus high sensitivities can be achieved in a quite small gas volume. As a result, a PAS or PTS instrument can be compact and robust [6].

As a rapidly developing photoacoustic technique, quartz-enhanced photoacoustic spectroscopy (QEPAS) was reported in 2002 for the first time [7]. In QEPAS, small-size, high-quality factor ( $Q$  factor), and low-cost quartz tuning forks (QTFs) are used as a transducer to sense the acoustic signal [8–12]. The modulated laser is focused between the QTF prongs, surrounded by the gas sample. Upon the absorption of laser energy from the target gas molecules, the acoustic waves generated by the photoacoustic effect drive the QTF prong to vibration. The QTF generated electrical signals via the piezoelectric effect [13–20].

In QEPAS, the QTF must be immersed in the gas samples to collect the acoustic signals. Therefore, the QEPAS technique cannot be used for remote sensing. In addition, due to the surface electrode of a commercial QTF being made of metal (silver or gold), the QEPAS technique is not recommended for corrosive gas sensing.

To overcome these shortcomings, a sister technique of QEPAS, quartz-enhanced photothermal spectroscopy (QEPTS), also named light-induced thermal-elastic spectroscopy (LITES), was developed by Y. Ma in 2018 [21]. Different from QEPAS, in LITES, the QTF was used as a photodetector [22,23]. The laser beam is modulated at the QTF resonance frequency or one of its overtones, then passes through a gas absorption cell and finally is focused on the surface of the QTF. Due to the thermoelastic effect of the quartz, the modulated absorbed thermal energy is converted into mechanical motion and then amplified by the QTF resonance. The advantage of LITES over QEPAS is that the QTF is no longer immersed in the target gas molecules. Thereby, LITES can be used for remote standoff sensing, combustion diagnostics, or corrosive gas detection.

To achieve high sensitivity in LITES, a high thermal-elastic effect of the QTF is necessary. From the previous experiments, the thermal-elastic performance of the QTF is closely related to laser excitation. For a commercial QTF, the best excitation was achieved by focusing the light beam on the surface of the QTF nearby the prongs base by normal incidence [24]. Custom QTFs with a special coating and lower resonance frequency can be employed to enhance the thermal-elastic conversion but cost hundreds of times more with respect to a standard 32-kHz QTF [25–27]. To date, the region at the base of the QTF prongs has been demonstrated to be the best area where the laser beam should be focused to achieve high thermal-elastic conversion [28], but only the internal regions, near to the prongs gap, have been exploited.

In this work, we propose a novel side-excitation light-induced thermoelastic spectroscopy (SE-LITES) implementing a custom 32-kHz QTF. The SE-LITES has two advantages: (i) an inner

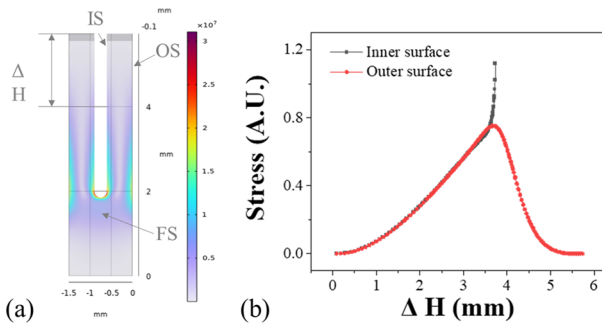


**Fig. 1.** (a) Stress distributions on the QTF surface.  $\Delta H$ , the distance between the QTF opening and laser incident point; IS, inner surface; OS, outer surface; FS, front surface. (b) Normalized stress on the QTF side surface as the function of  $\Delta H$ . Black square symbols, QTF prong IS; Red dot symbols, QTF prong OS.

surface-excitation approach to achieve a thermoelastic effect; (ii) increased optical path length. The proposed SE-LITES enhances the detection sensitivity of LITES by more than one order of magnitude.

First, the elastic stress on the 32-kHz QTF surface was analyzed by the finite element method (FEM) using COMSOL Multiphysics software. It was observed that the stress on the QTF prong side surface was higher than that on the central prong surface (front surface, FS), as shown in Fig. 1(a). Therefore, the maximum thermoelastic effect should be achieved by focusing the laser beam on the side surfaces. The normalized inner and outer surface stress as the function of  $\Delta H$ , defined as the distance from the QTF base, is plotted in Fig. 1(b). Both the stress on the QTF prong inner surface and outer surface increased with the increase of  $\Delta H$ , reaching the maximum value at  $\sim 3.8$  mm, corresponding to the prong/base contact region of the QTF. The maximum stress value on the inner surface was 47% higher than that on the outer surface.

The thermoelastic effect can be described by Eqs. (1) and (2) as follows [29]:

$$\frac{\partial^2 u}{\partial x^2} - \frac{1}{v^2} \frac{\partial^2 u}{\partial t^2} = \beta \frac{\partial T}{\partial x}, \quad (1)$$

$$\frac{\partial T}{\partial t} = \frac{K}{\rho C} \frac{\partial^2 T}{\partial x^2} + \frac{p}{\rho C}, \quad (2)$$

where  $u$ ,  $T$ ,  $\beta$ , and  $v$  are the elastic amplitude, temperature, thermal expansion coefficient, and elastic wave velocity, respectively. Additionally,  $K$ ,  $\rho$ ,  $C$ , and  $p$  are the thermal conductivity, density, heat capacity, and power absorption, respectively.

According to the above-mentioned theory, the QTF thermoelastic amplitude is closely related to the optical power absorption. The schematic diagram of side-excitation light-induced thermoelastic spectroscopy approach (SE-LITES) is shown in Fig. 2(a). A standard QTF usually has a quadrupole electrode pattern with the four surfaces of the QTF prong covered by silver film electrode patterns. In LITES, the areas covered by a silver film cannot be used since they will strongly reflect the laser beam, preventing the absorption of optical power. Thereby, for the proposed SE-LITES, one of the silver film electrodes on the QTF prong outer surface was removed while keeping the others untouched, resulting in an electrode-modified QTF, as shown in Fig. 2(b). The silver electrode was removed by chemical etching with 65% nitric acid at room temperature and atmospheric pressure for 5 min. A custom-made mask was

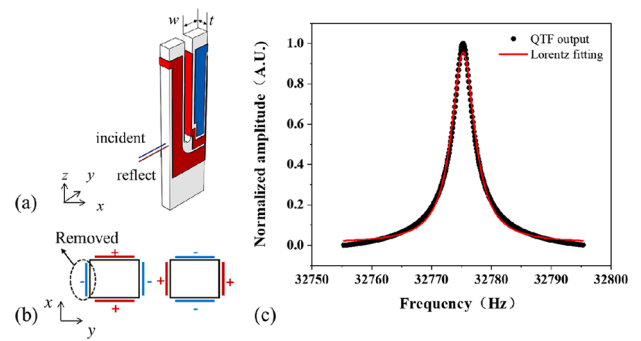


**Fig. 2.** (a) Schematic diagram of SE-LITES. Here,  $w = 0.6$  mm is the prong width, while  $t = 0.3$  mm is the QTF crystal thickness. (b) Top view of a QTF electrode. (c) Resonance curve of the electrode-modified QTF.

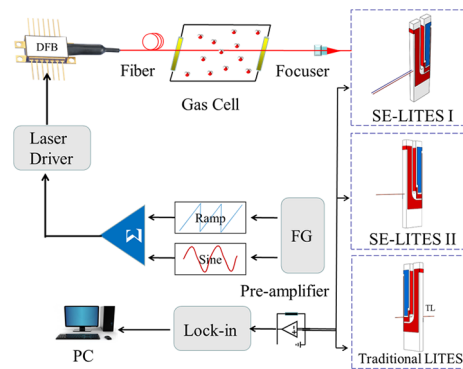


**Fig. 3.** Schematic of the SE-LITES setup. FG, function generation;  $\Sigma$ , adder; PC, personal computer; Lock-in, lock-in amplifier. SE-LITES I is dual-excitation at Point B, see Fig. 4 (a); SE-LITES II is single-excitation at Point C, see Fig. 4 (a).

to control the corroded area. After removal, the QTF surface was flushed with acetone and cleaned by an air duster. Once the silver film electrode was removed, the laser beam was now able to be transmitted inside the QTF crystal and absorbed from the back silver/chromium layer, allowing excitation of the QTF prong inner surface, thus enhancing the thermoelastic effect. For the portion of light reflected by the inner surface, the possible absorption path inside the quartz crystal for SE-LITES was  $2w \approx 1.2$  mm, improved by 4 times with respect to the absorption path for standard LITES corresponding to the QTF crystal thickness  $t \approx 0.3$  mm.

The resonance curve of the electrode-modified QTF is shown in Fig. 2(c). A resonance frequency of 32,775 Hz with a full width at half maximum (FWHM) of  $\sim 2.7$  Hz, resulting in a  $Q$  factor value of  $\sim 12,000$ , was measured. The  $Q$  factor was typical of a standard QTF, demonstrating that the silver pattern modification has not impacted on the QTF performance. Next, the SE-LITES was evaluated by the experimental setup depicted in Fig. 3. As a proof of concept, a 1.39- $\mu\text{m}$  near-infrared fiber coupled distributed feedback (DFB) diode laser was employed as the excitation source. Water vapor in the ambient air was selected as the gas target. A laser diode driver (Thorlabs CLD1015) was employed to control the temperature and injection current of the diode laser. The wavelength modulation technique was used to increase the detection sensitivity. A ramp signal with a period

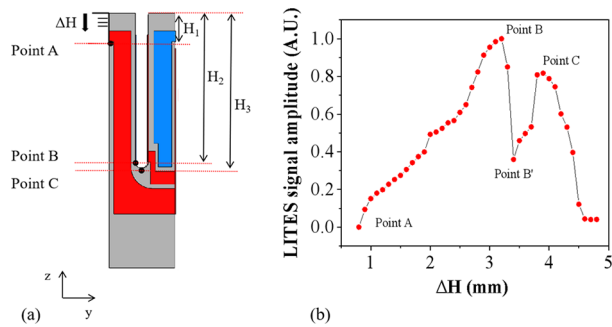


**Fig. 4.** (a) Diagram of laser incident position for SE-LITES. (b) LITES signal amplitude as a function of  $\Delta H$ .

of 400 s and a sine signal with a frequency of  $f_0/2$  was generated by a function generator (Tektronix AFG3102), where  $f_0$  is the resonance frequency of the QTF. The laser temperature was set to 17.6°C. The injection current was changed from 42 mA to 54 mA, corresponding to a laser emission wavelength spanning from  $7194.4 \text{ cm}^{-1}$  to  $7195.1 \text{ cm}^{-1}$ . An  $\text{H}_2\text{O}$  absorption line located at  $7194.8 \text{ cm}^{-1}$  with the intensity of  $3.2 \times 10^{-21} \text{ cm/mol}$  was targeted, according to the HITRAN database. The laser beam was collimated through a gas cell and then focused on the side of the QTF by a gradient-index (GRIN) lens. The focal length of the GRIN lens was 11 mm and the diameter of the beam waist was  $\sim 100 \mu\text{m}$ . The length of the gas absorption cell is 30 cm. The output electrical signal from the QTF was amplified by a custom trans-impedance preamplifier with a 10-M $\Omega$  feedback resistor. A lock-in amplifier (Stanford SR830) was used to demodulate the signal in a  $2f$  mode. A LabView program was used to control the system and calculate the  $\text{H}_2\text{O}$  vapor concentration.

The laser spot incident position was optimized to maximize the thermoelastic amplitude in SE-LITES. By changing the laser focal spot position on the QTF, the corresponding LITES signal amplitudes were recorded, as shown in Fig. 4. In particular, points A, B, and C, corresponding to the end of the positive electrode (red), the end of the negative electrode (blue), and the junction point of the QTF prong, respectively, are marked in Fig. 4. The related  $\Delta H$  values:  $\Delta H = H_1$ ,  $\Delta H = H_2$ , and  $\Delta H = H_3$  are also highlighted in Fig. 4. The laser focal spot position was scanned from Point A to Point C along the  $z$  direction. When  $H_1 < \Delta H < H_2$ , the LITES signal amplitude increases monotonously with  $\Delta H$ . A peak value was obtained at Point B, where  $\Delta H = 3.1 \text{ mm}$ . This can be attributed to an optimal excitation of QTF. From point B to point C, there is no silver film coating on the prong's inner surface and also the optical path length in the crystal rapidly decreases. Thereby, the LITES signal decreases reaching a minimum at  $\Delta H = 3.4 \text{ mm}$  [point B' in Fig. 4(b)]. Then moving toward Point C, the optical absorption path increased gradually and the LITES signal amplitude rises accordingly. As a result, another peak value was achieved at Point C, where  $\Delta H = 3.8 \text{ mm}$ . Beyond Point C, the thermoelastic effect in this area is less sensitive (see Fig. 1), and the LITES signal decreased gradually.

The modulation depth has a significant impact on the thermoelastic effect and thus the laser wavelength modulation depth must be optimized. The LITES  $2f$  signal amplitudes measured for different modulation depths are shown in Fig. 5(a). The

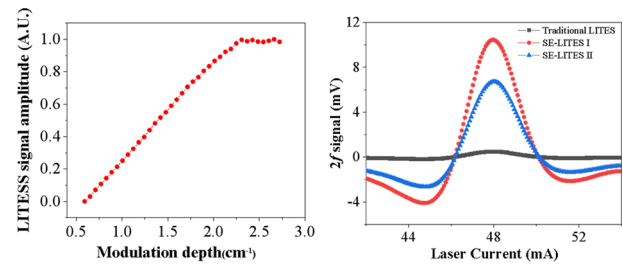


**Fig. 5.** (a) SE-LITES signal amplitude as a function of modulation depth. (b)  $2f$  signal comparison of SE-LITES and traditional LITES.

**Table 1.** The  $2f$  Signal,  $1\sigma$  Noise, and Minimum Detection Limit Obtained by Three Different LITES Systems

	Signal/mv	Noise/ $\mu\text{v}$	SNR	MDL/ppm
SE-LITES I	10.45	2.95	3540	3.96
SE-LITES II	6.73	2.52	2667	5.25
Traditional LITES	0.48	1.96	246	56.98

LITES signal amplitude increases monotonously up to a modulation depth of  $2.3 \text{ cm}^{-1}$ , while after this value, a plateau is observed. Thereby, the optimal value results are  $2.3 \text{ cm}^{-1}$ .

With the optimized laser focal position and modulation depth, the LITES  $2f$  signals obtained by SE-LITES and traditional LITES were compared. Figure 5(b) shows the  $2f$  signals obtained by SE-LITES I (incidence point B), SE-LITES II (incidence point C), and traditional LITES. The  $2f$  signal peaks obtained by SE-LITES I and SE-LITES II were 10.45 mV and 6.73 mV, respectively, while the amplitude obtained by traditional LITES was only 0.48 mV. The background noise level of each sensor was measured when the laser was far away from the absorption line of water. The results are summarized in Table 1. Compared with the traditional LITES system, the SE-LITES improved the detection SNR by more than 1 order of magnitude. With the SE-LITES I, the signal amplitude and SNR were enhanced by  $\sim 22$  times and  $\sim 15$  times. Considering a signal-to-noise ratio (SNR) of 3540, a normalized noise equivalent absorption (NEEA) coefficient of  $1.84 \times 10^{-9} \text{ W}\cdot\text{cm}^{-1}\cdot\text{Hz}^{-1/2}$  was achieved.

In conclusion, we reported on a side-excitation light-induced thermoelastic spectroscopy (SE-LITES) method. The silver electrode pattern of a commercial QTF was modified to realize the SE-LITES setup. The modification of electrode, making a window on the QTF surface, allows the incidence of the laser beam. The other electrodes were remained and fully used as a laser absorption layer. Benefiting from the inner surface excitation, the thermoelastic effect was enhanced. Compared to traditional LITES, the detection SNR was enhanced by more than one order of magnitude. In this work, the whole side electrode was removed to explore the optimal excitation position of the laser. With the side electrode removed, the resonance amplitude of the QTF was slightly decreased. Further improvement can be made by opening a micro aperture on the QTF prong outer surface to minimize the impact of electrode modification. This work proposed a novel and sensitive light detector based on thermoelastic effects, which will greatly benefit the infrared detection technology.

**Funding.** National Key Research and Development Program of China (2021YFB2800801, 2019YFE0118200); National Natural Science Foundation of China (12174156, 12174155, 62105125, 62005105, 62075088, 62175137); Natural Science Foundation of Guangdong Province (2020B1515020024, 2019A1515011380); Key-Area Research and Development Program of Guangdong Province (2019B010138004); Special Project in Key Fields of the Higher Education Institutions of Guangdong Province (2020ZDZX3022); the Science and Technology Projects of Guangzhou (202102020445); Foundation for Distinguished Young Talents in Higher Education of Guangdong (2018KQNCX009); Chinese Aeronautical Establishment (201808W4001); Project of Guangzhou Industry Leading Talents (CXLJTD-201607); Fundamental Research Funds for the Central Universities (21619402, 11618413); State Key Laboratory of Applied Optics (SKLAO-201914).

**Disclosures.** The authors declare no conflicts of interest.

**Data availability.** Data underlying the results presented in this paper are not publicly available at this time but may be obtained from the authors upon reasonable request.

## REFERENCES

1. K. Krzemppek, A. Hudzikowski, A. Gluszek, G. Dudzik, K. Abramski, G. Wysocki, and M. Nikodem, *Appl. Phys. B* **124**, 74 (2018).
2. C. Feng, M. Giglio, B. Li, A. Sampaolo, P. Patimisco, V. Spagnolo, L. Dong, and H. Wu, *Molecules* **27**, 6505 (2022).
3. K. Krzemppek, G. Dudzik, and K. Abramski, *Opt. Express* **26**, 28861 (2018).
4. X. Yin, H. Wu, L. Dong, B. Li, W. Ma, L. Zhang, W. Yin, L. Xiao, S. Jia, and F. K. Tittel, *ACS Sens.* **5**, 549 (2020).
5. Y. Ma, S. Qiao, Y. He, Y. Li, Z. Zhang, X. Yu, and F. K. Tittel, *Opt. Express* **27**, 14163 (2019).
6. D. Marchenko, A. H. Neerincx, J. Mandon, J. Zhang, M. Boerkamp, J. Mink, S. M. Cristescu, S. T. L. Hekkert, and F. J. M. Harren, *Appl. Phys. B* **118**, 275 (2015).
7. A. A. Kosterev, Y. A. Bakhrkin, R. F. Curl, and F. K. Tittel, *Opt. Lett.* **27**, 1902 (2002).
8. A. Sampaolo, P. Patimisco, M. Giglio, A. Zifarelli, H. Wu, L. Dong, and V. Spagnolo, *Anal. Chim. Acta* **1202**, 338894 (2022).
9. Q. Wu, H. Lv, L. H. Wu, M. Giglio, W. Zhu, Y. Zhong, A. Sampaolo, P. Patimisco, L. Dong, V. Spagnolo, J. Yu, and H. Zheng, *Opt. Lett.* **47**, 4556 (2022).
10. Y. F. Ma, *Appl. Sci.* **8**, 1822 (2018).
11. M. Köhring, A. Pohlkötter, U. Willer, M. Angelmahr, and W. Schade, *Appl. Phys. B* **102**, 133 (2011).
12. H. Lv, H. Zheng, Y. Liu, Z. Yang, Q. Wu, H. Lin, B. A. Z. Montano, W. Zhu, J. Yu, R. Kan, Z. Chen, and F. K. Tittel, *Opt. Lett.* **46**, 3917 (2021).
13. Y. Ma, S. Qiao, P. Patimisco, A. Sampaolo, Y. Wang, F. K. Tittel, and V. Spagnolo, *Appl. Phys. Lett.* **116**, 061101 (2020).
14. H. Zheng, Y. Liu, H. Lin, B. Liu, D. Li, B. Huang, Y. Wu, L. Dong, W. Zhu, J. Tang, H. Guan, H. Lu, Y. Zhong, J. Fang, Y. Luo, J. Zhang, J. Yu, and F. K. Tittel, *Photoacoustics* **17**, 100158 (2020).
15. H. Wu, L. Dong, X. Yin, A. Sampaolo, P. Patimisco, W. Ma, L. Zhang, W. Yin, L. Xiao, V. Spagnolo, and S. Jia, *Sens. Actuators, B* **297**, 126753 (2019).
16. Y. Liu, H. Lin, B. A. Z. Montano, W. Zhu, Y. Zhong, R. Kan, B. Liu, J. Yu, M. Shao, and H. Zheng, *Photoacoustics* **25**, 100332 (2022).
17. M. Giglio, A. Elefante, P. Patimisco, A. Sampaolo, F. Sgobba, H. Rossmadl, V. Mackowiak, H. Wu, F. K. Tittel, L. Dong, and V. Spagnolo, *Opt. Express* **27**, 4271 (2019).
18. J. P. Waclawek, H. Moser, and B. Lendl, *Opt. Express* **24**, 6559 (2016).
19. C. Lou, H. Chen, X. Li, X. Yang, Y. Zhang, J. Yao, Y. Ma, C. Chang, and X. Liu, *Opt. Express* **29**, 20190 (2021).
20. H. Lin, H. Zheng, B. A. Z. Montano, H. Wu, M. Giglio, A. Sampaolo, P. Patimisco, W. Zhu, Y. Zhong, L. Dong, R. Kan, J. Yu, and V. Spagnolo, *Photoacoustics* **25**, 100321 (2022).
21. Y. Ma, Y. He, Y. Tong, X. Yu, and F. K. Tittel, *Opt. Express* **26**, 32103 (2018).
22. T. Wei, A. Zifarelli, S. D. Russo, H. Wu, G. Menduni, P. Patimisco, A. Sampaolo, V. Spagnolo, and L. Dong, *Appl. Phys. Rev.* **8**, 041409 (2021).
23. Y. Ma, C. Zheng, L. Hu, K. Zheng, F. Song, Y. Zhang, Y. Wang, and F. K. Tittel, *Sens. Actuators, B* **370**, 132429 (2022).
24. Y. He, Y. Ma, Y. Tong, X. Yu, and F. K. Tittel, *Opt. Lett.* **44**, 1904 (2019).
25. Y. Ma, Y. He, P. Patimisco, A. Sampaolo, S. Qiao, X. Yu, F. K. Tittel, and V. Spagnolo, *Appl. Phys. Lett.* **116**, 011103 (2020).
26. S. Qiao, Y. Ma, Y. He, P. Patimisco, A. Sampaolo, and V. Spagnolo, *Opt. Express* **29**, 25100 (2021).
27. S. Qiao, A. Sampaolo, P. Patimisco, V. Spagnolo, and Y. Ma, *Photoacoustics* **27**, 100381 (2022).
28. S. Qiao, Y. He, and Y. Ma, *Opt. Lett.* **46**, 2449 (2021).
29. R. J. von Gutfeld, *Ultrasonics* **18**, 175 (1980).